British Journal of Cancer

ARTICLE

Check for updates

Cellular and Molecular Biology

Peroxiredoxin-1 Tyr194 phosphorylation regulates LOX-dependent extracellular matrix remodelling in breast cancer

Shireen Attaran[1,2], John J. Skoko[1,2], Barbara L. Hopkins[2,3], Megan K. Wright[4], Laurel E. Wood[1], Alparslan Asan[1,2], Hyun Ae Woo[5], Adam Feinberg[6] and Carola A. Neumann[1,2]✉

BACKGROUND: Peroxiredoxin 1 (PRDX1) belongs to an abundant family of peroxidases whose role in cancer is still unresolved. While mouse knockout studies demonstrate a tumour suppressive role for PRDX1, in cancer cell xenografts, results denote PRDX1 as a drug target. Probably, this phenotypic discrepancy stems from distinct roles of PRDX1 in certain cell types or stages of tumour progression.
METHODS: We demonstrate an important cell-autonomous function for PRDX1 utilising a syngeneic mouse model (BALB/c) and mammary fibroblasts (MFs) obtained from it.
RESULTS: Loss of PRDX1 in vivo promotes collagen remodelling known to promote breast cancer progression. PRDX1 inactivation in MFs occurs via SRC-induced phosphorylation of PRDX1 TYR194 and not through the expected direct oxidation of CYS52 in PRDX1 by ROS. TYR194-phosphorylated PRDX1 fails to bind to lysyl oxidases (LOX) and leads to the accumulation of extracellular LOX proteins which supports enhanced collagen remodelling associated with breast cancer progression.
CONCLUSIONS: This study reveals a cell type-specific tumour suppressive role for PRDX1 that is supported by survival analyses, depending on PRDX1 protein levels in breast cancer cohorts.

British Journal of Cancer (2021) 125:1146–1157; https://doi.org/10.1038/s41416-021-01510-x

INTRODUCTION

Breast cancer is one of the most common malignant diseases in US women, with over 279,100 new cases and over 42,690 deaths expected in 2020 alone [1]. In these patients, it is not the primary tumour, but predominantly the metastases to distant sites in the body, and extrinsic factors provided by other cell types within the tumour–stroma, that ultimately proves fatal. Within the tumour, fibroblasts frequently constitute the bulk of tumour-associated cells, contribute to oncogenesis and promote metastasis [2–4]. Fibroblasts are one of the most abundant cell types in connective tissues and regulate tissue homoeostasis under normal conditions. During tissue injury, reactive oxygen species (ROS), such as hydrogen peroxide (H_2O_2), growth factors and cytokines are released that activate fibroblasts to transition into myofibroblasts [5]. Myofibroblasts then facilitate the bulk of the wound healing by deposition of matrix proteins (collagen, elastin, etc.) and secretion of enzymes that facilitate matrix contraction (matrix metalloproteinases, lysyl oxidases etc.). Once the wound is healed, myofibroblast activation stops, and they undergo apoptosis [6]. During wound healing, fibroblasts in cancer tissue undergo transitions to myofibroblasts and cancer-associated fibroblasts (CAFs), however, unlike normal wound healing, CAFs are perpetually exposed to cytokines and growth factors secreted by the tumour microenvironment resulting in constant extracellular matrix (ECM) remodelling. Therefore, tumours are commonly referred to as wounds that do not heal because of aberrant wound healing responses [7, 8].

Lysyl oxidase (LOX) and it's family members the LOX-like proteins LOXL1-4 are copper-dependent amine oxidases, which oxidise the ε-amino group of the peptidyl lysine to peptidyl aldehydes of ECM proteins such as collagen. This enzymatic activity enables LOX to cross-link collagen monomers to dimers, trimers and higher-order oligomers to build the tensile strength of cancer tissues [9]. LOX enzymes are secreted as proenzymes (proLOX) that are proteolytically processed in the extracellular milieu to release the propeptide that produces mature, active LOX [10]. The exact mechanisms regulating LOX secretion are still unclear.

Peroxiredoxin (PRDX) proteins are intracellular peroxidases that are highly sensitive to alterations in H_2O_2 concentrations [11]. PRDX proteins can coordinate cell signalling via direct ROS scavenging or by acting as a redox sensor that enables control of binding partner activity [12]. Currently, six mammalian family members are known, out of which, only PRDX1 suppresses breast cancer formation in mice through the protection of PTEN phosphatase from oxidation-induced inactivation [13, 14]. We have recently shown that PRDX1 loss in mammary fibroblasts

[1]Department of Pharmacology & Chemical Biology, University of Pittsburgh, Pittsburgh, PA, USA. [2]Women's Cancer Research Center, UPMC Hillman Cancer Center, Pittsburgh, PA, USA. [3]Department of Human Genetics, University of Pittsburgh, Pittsburgh, PA, USA. [4]University of Pittsburgh, School of Medicine, Pittsburgh, PA, USA. [5]College of Pharmacy, Graduate School of Pharmaceutical Sciences, Ewha Womans University, Seoul, Republic of Korea. [6]Department of Materials Science and Engineering and Biomedical Engineering, Carnegie Mellon University, Pittsburgh, PA, USA. ✉email: neumannc@upmc.edu

Received: 19 January 2021 Revised: 22 June 2021 Accepted: 21 July 2021
Published online: 13 August 2021

mimics the activated phenotype found in cancer-associated fibroblasts (CAFs) that includes enhanced migratory and invasive properties and upregulation of fibroblast associated protein (FAP) and α-smooth muscle actin (α-SMA) [15]. Loss of function of PRDXs proteins in cancer is rarely due to genomic alteration, suggesting posttranslational modifications (PTM) as main regulators [12]. Oxidation of the peroxidatic cysteine residue of PRDX1 proteins is the classical PTM that has been recognised to modulate downstream signalling cascades, but increasing evidence supports that dynamic changes to phosphorylation of PRDX proteins are also an important determinant in redox signalling [12].

The underlying mechanisms of fibroblast contribution to cancer invasiveness are still elusive. Given the role of PRDX1 in the context of cancer development and their role in inhibiting the transition of mammary fibroblasts into CAFs, the breast cancer cell fibroblast crosstalk mediated by mammary fibroblast PRDX1 at the tumour–stroma interface was investigated. Here, under conditions resembling physiological relevant oxygen concentration (5%), we demonstrate a novel mechanism that participates in ECM remodelling by which PRDX1 can become inactivated via SRC-kinase phosphorylation through a paracrine loop from cancer cell-secreted factors, thereby mediating PRDX1-dependent collagen remodelling through LOX enzymes.

MATERIALS AND METHODS

Syngeneic mouse model of breast cancer

All animal studies were approved by the University of Pittsburgh IACUC (protocol #: 18093443). A BALB/c syngeneic mouse model was designed to evaluate tumour growth and ECM remodelling in vivo. Knockdown PRDX1 MFs were generated through the expression of 3′ UTR-targeted shPRDX1 [15]. Immune-competent BALB/c MFs (shPrdx1 or control vector) expressing iRFP were co-injected with GFP+ 67NR cells into the right and left 4th inguinal mammary fat pad of 8-week-old female BALB/c mice ($n = 4$ per group, per timepoint; six groups in total). The 67NR cell line is a subpopulation line isolated from a spontaneously arising mammary tumour from a BALB/cfC3H mouse. This cell line is highly tumorigenic but very rarely spontaneously metastasises [16]. After 1-, 2- or 4-week post injection, mice were euthanized by CO_2 exposure and mammary glands were harvested then fixed in 2% paraformaldehyde for 2 h and subsequently stored in 0.02% sodium azide-PBS solution. Mammary glands were harvested and fixed at the same time for each group. Following fixation, tissues were imaged using second-harmonic generation (SHG) and multiphoton microscopy (MPM). Two glands per mouse were analysed, eight total per group.

Second-harmonic generation (SHG) and multiphoton microscopy (MPM)

Collagen has the unique property, based on its chemistry and its triple-helical structure, that allows for label-free imaging using second-harmonic generation (SHG) contrast on a multiphoton microscope [17]. An Olympus FV1000 with multiphoton excitation (Tokyo, Japan) equipped with a Spectra-Physics DeepSee Mai Tai Ti–Sapphire laser (Newport, Mountain View, CA) with a 1.12NA 259 MPE water immersion objective was used to visualise collagen, iRFP and GFP.

Collagen quantification in mouse mammary glands

Collagen deposition was quantified using ImageJ. A z-projection of 40 slices was maximally projected in an 8-bit image of the collagen only channel and locations of high tumour load (green) were quantified for collagen intensity in week-1 and -2-injected mammary glands.

CT-FIRE and curve align collagen architecture assessment

Collagen fibres were identified from SHG images using the CT-FIRE software package (loci.wisc.edu/software/ctFIRE, v.2.0b). Further analysis of fibre-to-fibre orientation was completed using the Curve-Align software package (loci.wisc.edu/software/curvealign, v.4.0b). Specifically, for collagen fibre length measurements, eight frames of four mice from each MF genotype (EV and shPRDX1) were analysed in total. The alignment coefficient ranges from 0 to 1, with 1 indicating perfectly aligned fibres, and smaller values representing more randomly distributed fibres. The alignment coefficient indicates the dispersity of the fibre orientations. Collagen fibre angle measurements quantify perpendicular collagen fibre arrangements at the tumour–stroma interface [18–20].

Fibroblast isolation and cell culture conditions

Primary MFs were isolated from female BALB/c mouse mammary glands and processed, as previously described [15]. Briefly, female BALB/c mice were purchased from Jackson laboratory. Animals were housed in a pathogen-free facility in accordance with the Animal Care and Use Guidelines of the University of Pittsburgh. Mammary stromal fibroblasts were isolated from 8 to 12-week-old virgin BALB/c female mice. Briefly, mice were sacrificed, and the mammary glands were quickly removed, washed twice in wash solution (46 mL Dulbecco's phosphate-buffered saline (DPBS) (Sigma), 2.5 mL FBS (Gibco), 100 units/ml penicillin, 100 mg/ml streptomycin (Mediatech) and 400 µL Fungizone), and finely minced. Tissues were then disaggregated by repeated aspiration using a 10-ml syringe (no needle). Tissues were then centrifuged and digested at 37 °C for 2 h in DMEM containing 10% FBS, 100 units/ml penicillin, 100 mg/ml streptomycin (Mediatech), 3500 units/ml collagenase followed by a 10 min trypsin digestion step that was neutralised with FBS. Cells were then washed twice in PBS and plated in complete DMEM with 5% FBS. After 2 h, non-adhered cells were removed and the remaining fibroblasts were cultured for several weeks at 37 °C in 5% CO_2 and 5% oxygen until spontaneously immortalised. Mammary fibroblasts, MDA-MB-231, MCF-7 and MDA-MB-468 cells were maintained in DMEM with 10% FBS and penicillin/streptomycin. BT-549 cells were maintained in RPMI-1640 with 10% FBS and penicillin–streptomycin. Cells were maintained at 37 °C in a 5% CO_2 and 5% O_2 incubator (ThermoFisher HeraCell 150i).

Lentivirus preparation and infection

Lentivirus of pLKO.1 shRNA vector specific to Prdx1 was prepared in 293T HEK cells in OPTI-MEM Reduced Serum Media. Lentiviral shRNA plasmids targeting mouse PRDX1 (Millipore-Sigma) were used to generate PRDX1-deficient MFs. Clone shPRDX1 #1 (NM_011034.2-558s1c1 5′- CCGGGCCTTCCAGTTCACTGACAAACTCGAGTTTGTCAGTGAACTGGAAGGCTTTTTG-3′), shPRDX1 #2 (NM_011034.2-246s1c1 5′- CCGGGCTTTCAGTGATAGAGCCGATCTCGAGATCGGCTCTATCACTGAAAGCTTTTTG-3′), shPRDX1 #3 (NM_011034.2-369s1c1 5′- CCGGCCCATGAACATTCCCTTAATACTCGAGTATTAAGGGAATGTTCATGGGTTTTTG-3′), shPRDX1 #4 (NM_011034.2-251s1c1 5′- CCGGCAGTGATAGAGCCGATGAATTCTCGAGAATTCATCGGCTCTATCACTGTTTTTG-3′).

Following 24 h, the media was exchanged to 10% FBS-DMEM media and the virus was collected at 24 and 48 h. Parental MFs were then infected with 8 µg/mL polybrene in the media. Following the initial 24 h infection, the media was exchanged, and 7 days post infection, cells were placed under a puromycin selection (2 µg/mL) in 10% FBS-DMEM media. Infrared-red fluorescent protein (iRFP) and green fluorescent protein (GFP) were expressed into control and shPrdx1 MFs via lentiviral infection. Cells were transduced with viral particles produced in HEK 293T cells from the lentiviral plasmid pLVX-EGFP-IRES-Hyg, as previously described [21]. Seven days post infection, iRFP and GFP-expressing MFs were placed under hygromycin selection and subsequently expanded.

In vitro collagen deposition assay

Parental MFs were plated in 48-well plates at a seeding density of 3×10^4 cells per well in DMEM media containing 10% FBS, 100 units/ml penicillin and 100 mg/ml streptomycin. Cells were incubated at 37 °C in a 5% CO_2 and 5% oxygen incubator for 6 days to allow for cellular crowding and collagen deposition. On day 6, cell layers were washed twice with 1× HBSS and collagen was extracted from cell layers via acidic porcine pepsin digestion, as described previously [22, 23]. Protein samples were separated using SDS-PAGE with a 7% acrylamide resolving gel, under non-reducing conditions. Protein bands were stained using the Silver Quest kit (Invitrogen).

Immunoblot

MFs were lysed in a tris lysis buffer (50 mM Tris; 2% Triton X-100; 0.5 mM EDTA; 0.5 mM EGTA; 150 mM NaCl; 10% glycerol; 50 mM NaF; 1 mM NaVO4; 40 mM β-glycerophosphate), supplemented with 30 µg/mL catalase from bovine liver (Sigma), and proteinase inhibitors. Protein concentrations were quantified using the Pierce BCA Protein Assay kit, according to the manufacturer's instructions (ThermoFisher). Whole-cell lysates were fractionated by SDS-PAGE and transferred to a nitrocellulose membrane according to the manufacturer instructions (BioRad). Membranes were blocked with 5%

BSA in TBS for 2 h, and incubated with antibodies against PRDX1 (1:1000, Abcam), PRDX-SO3 (1:1000, Abcam), or Phospho-PRDX1 Tyr194 (1:1000, Cell Signaling) and GAPDH (1:1000) (Abcam), overnight at 4 °C. Membranes were washed three times for 10 min in TBST (0.05% Tween-20) and visualised by IR detection. For IR processing, membranes were incubated with a 1:15,000 dilution of anti-goat, anti-rabbit, or anti-mouse IRDye (LI-COR), for 30 min at 25 °C. Blots were washed with TBST three times and with TBS once, and imaged on an Odyssey (LI-COR) imager.

Immunoprecipitations

HEK 293T cells (5×10^5) were transiently transfected with 2 µg pcDNA3-FLAG-LOX1 and pcDNA3-FLAG-LOXL2 plasmids, using the Fugene 6 system for 48 h. Cells were serum-starved for 30 min, then treated with 100 µM H_2O_2 for 30 min. Prior to lysis, cells were washed one time with PBS containing 20 mM of NEM (N-ethylmaleimide) to avoid oxidation of free thiols. Samples were lysed using a tris lysis buffer (50 mM Tris; 2% Triton X-100; 0.5 mM EDTA; 0.5 mM EGTA; 150 mM NaCl; 10% glycerol; 50 mM NaF; 1 mM NaVO4; 40 mM β-glycerophosphate), supplemented with 30 µg/ml catalase from bovine liver (Sigma), and proteinase inhibitors. Protein concentrations were quantified using the Pierce BCA Protein Assay kit, according to the manufacturer's instructions (Thermo). In all, 1 mg of cell lysate was incubated with 20 µL of acid-treated Anti-FLAG M2 Affinity Gel (Sigma) and 400 µL lysis buffer, at 25 °C for 3 h, with rotation. Precipitated samples were collected and washed four times with lysis buffer, and once with 1× TBS. Beads were boiled in Laemmli sample buffer (BioRad) in the presence or absence of β-mercaptoethanol (Sigma) for 10 min. In total, 20 µg of whole-cell lysate was prepared in Laemmli sample buffer as above for 5 min.

LOX secretion

Scramble and knockdown MFs were plated at a density of 1×10^5 cells per 10-cm plate. Cells were serum-starved in DMEM for 24 h. Following the 24 h starve, conditioned media was collected and secreted proteins were precipitated by trichloroacetic acid (TCA) precipitation as previously described [24]. Following TCA treatment, precipitates were washed twice with acetone and allowed to air dry for 10 mins. Pellets were then resuspended in 20 µl 2× Laemlli sample buffer and prepared for SDS-PAGE. LOX bands were detected with the anti-LOX Rabbit antibody (ab31238, Abcam) which reacts with the mature cleaved product of about 32 kDa.

Generation of mutants

PRDX1 mutant plasmids were generated by PCR amplification of plasmids generously donated by Dr. Hyun Ae Woo [25] with custom primers harbouring EcoRI (5′-GTCGAGAATTCATGTCTTCAGGAAATGCT-3′) and Bam HI (5′- GCTGGATCCTCACTTCTGCTTGGA-3′) restrictions sites. The PCR fragments were then digested and ligated into the pLVX plasmid. Lentiviral transduction of MFs was performed as indicated above.

Preparation of conditioned medium and treatment of MFs

All human breast cancer cell lines were purchased from ATCC. Human breast cancer cells were plated at a density of 1.0×10^6 per 10-cm^2 dish and incubated overnight in a 37 °C, 5% CO_2 and 5% oxygen incubator for 24 h then starved with serum-free DMEM for 48 h. Conditioned media was filtered through a 0.45-µm syringe filter then added to MFs.

Scramble or shPrdx1 MFs were seeded at a density of 5×10^5 cells per 10 cm^2 plate and incubated overnight at 37 °C with 5% CO_2 and 5% O_2. To measure MFs phosphorylation levels, cells were treated with MDA-MB-231 conditioned media for 30 min. For experiments with the SRC inhibitor PP1, cells were pretreated for 2 h with 20 µM PP1 and subsequently treated with conditioned media. Cells were then processed for immunoblotting. When measuring the effect of conditioned media on LOX secretion, MFs were incubated with conditioned media for 24 h and the supernatant was precipitated with 10% TCA and 0.4 mg/ml sodium deoxycholate and processed as indicated above.

RESULTS

PRDX1 regulates extracellular collagen remodelling

Oxidants such as hydrogen peroxide (H_2O_2) are an essential contributor in the transition of normal fibroblasts into CAFs thus enacting field cancerization that triggers not only cancer progression but also the de novo activation of CAFs [2, 26–31]. We recently reported that the peroxidase PRDX1 decreases ROS and inhibits a CAF-like phenotype in MFs [15]. To examine this PRDX1-controlled phenotype in vivo, a syngeneic mouse model of breast cancer was used. MFs were harvested from 1-week-old female BALB/c mice and allowed to spontaneously immortalise in 5% O_2 tissue culture conditions before viral transduction with iRFP and four targeting shPRDX1s. Clones shPRDX1–2 and shPRDX1-4 exhibited >90% knockdown and were chosen for further studies (Supplementary Fig. S1A). In a syngeneic mouse model (Fig. 1a), shPRDX1-4 or EV MFs were injected into fat pads of 8-week-old female BALB/c mice together with GFP+ 67NR breast cancer cells described as non-invasive [16]. Mammary glands were harvested, fixed and imaged by multiphoton microscopy in Z-projections after weeks 1 and 2. Collagen has the unique property, based on its chemistry and triple-helical structure, that allows for label-free imaging using second-harmonic generation (SHG) contrast on a multiphoton microscope [17]. Multiphoton imaging revealed quantitative and architectural differences in extracellular collagen between shPRDX1 and EV MFs tumours. First, intratumoral collagen was quantified by measuring the SHG signal within a Z-stacked bounding box (Supplementary Fig. S1B) that overlapped with a GFP+ 67NR cell-positive volume in the green channel using ImageJ. Figure 1c and Supplementary Fig. S1C demonstrate that tumoral collagen was significantly higher in samples with shPrdx1 MFs compared to EV MFs after 1 week of growth. Tumour samples with shPRDX1 MFs also trended towards increased collagen fibres after 2 weeks of growth. Next, automated segmentation and quantification software (CT-Fire, [20]) was used to analyse collagen fibre length, alignment coefficient (a measure of similarity between fibre orientations, by calculating the vector sum of absolute fibre angles) and the distribution of fibre angles (a measure of collagen fibres perpendicular to the tumour) [18, 19]. All three parameters have prognostic values in multiple cancers, including breast [18, 32]. Decreased PRDX1 expression in MFs significantly increased the number of collagen fibres with a length between 100 and 200 µm by 1.5% (EV MFs 2.1% and shPRDX1 MFs 3.6%) and longer than 200 µm by 3.9% (EV MFs 11.6% and shPRDX1 MFs 15.5%) (Fig. 1c, d). No significant differences were observed in fibre length up to 99.9 µm. Notably, alignment coefficient (Fig. 1e), and the perpendicular distribution of fibre angles around tumours (Fig. 1f, g) differed significantly between EV MFs and shPRDX1 MFs, where angles between 42.6 and 87.5° differed the most, suggesting an increased aligned perpendicular fibre arrangement when shPRDX1 MFs were co-transplanted with breast cancer cells compared to EV MFs. The distribution of fibre angles was further analysed by the tumour-associated collagen signature (TACS) system established in the Keely laboratory that correlates CT-FIRE predicted fibre angles to predict breast cancer patient outcome [18, 33]. As Supplementary Fig. S1D shows, 89% of shPrdx1-4 MFs-injected mammary glands showed TACS-3 grading, compared to 44% in the EV MF-injected mammary glands. Notably, tumour sizes per mammary gland did not significantly differ between shPRDX1 and EV MFs (Fig. 1h).

Collagen remodelling is the stimulation of new collagen production and tightening/rearranging of existing collagen fibres is a process described as cross-linking. To clarify the functional involvement of PRDX1 in collagen remodelling in more detail, low- and high-molecular-weight forms of collagen present in confluent monolayers of MFs were compared. Confluent shPRDX1 and control MFs were allowed to deposit collagen over a period of 6 days which after a pepsin digest, was analysed by non-reducing SDS-PAGE to separate non-cross-linked from cross-linked collagen (Fig. 1i). Cross-linking of two α-collagen chains between triple-helical domains results in the formation of pepsin-resistant β-dimers of collagen (β11, β12). Protein bands were visualised by silver staining [22, 23]. Confluent monolayers of PRDX1-deficient MFs increased levels of β11 and β12 cross-linked collagen by 56-fold (PRDX1 sh2) and 24-fold (PRDX1 sh4) compared to control MFs. Elevated levels of α1 and α2 non-cross-linked collagen (about

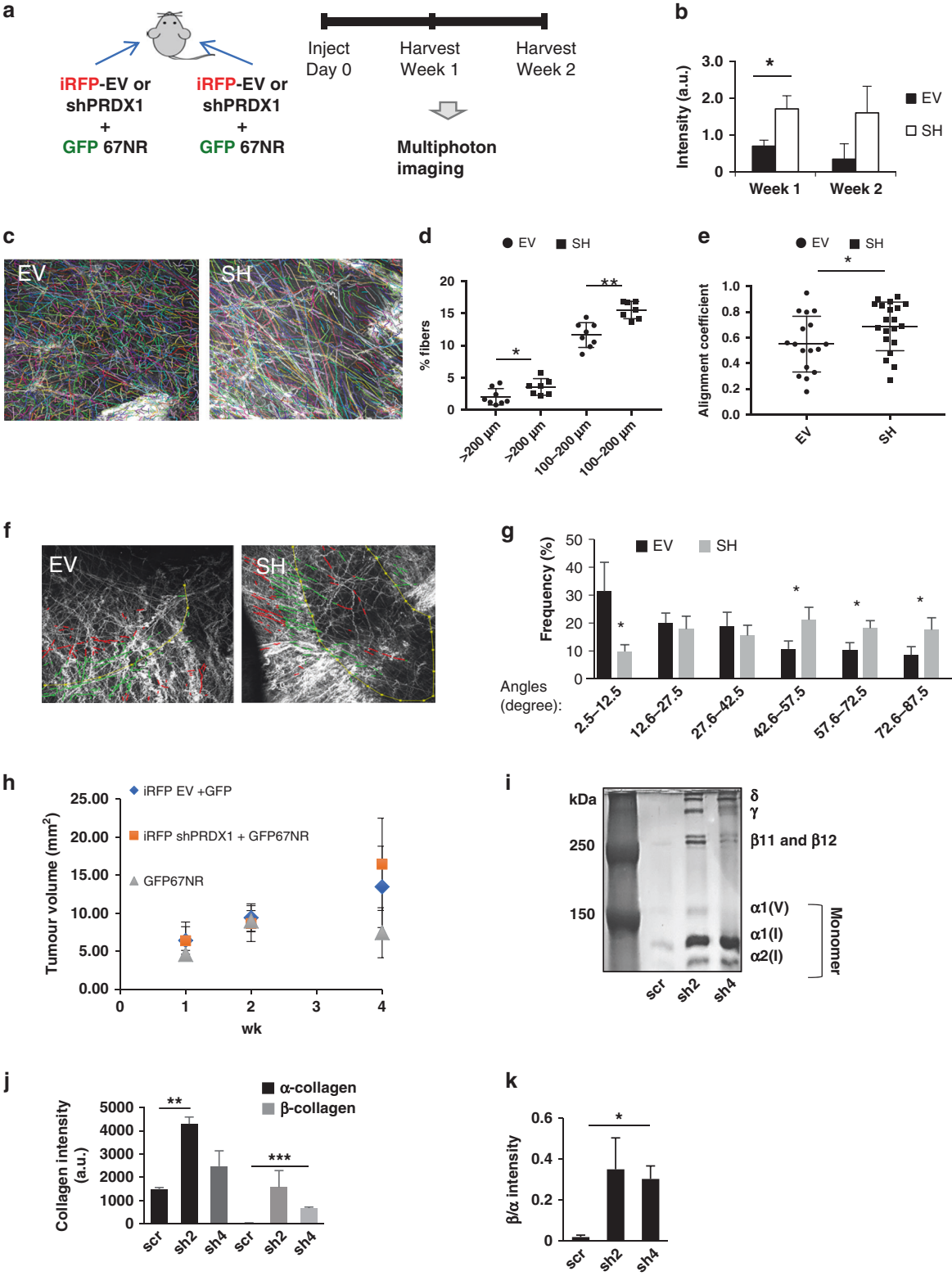

threefold for sh2 and 1.7-fold sh4) were also seen compared to control MFs, which is in agreement with our previous report of increased collagen in shPrdx1 MFs (Fig. 1j) [15]. This increased collagen deposition by shPRDX1 MFs translated into a higher ratio of cross-linked vs non-cross-linked collagen chains where shPRDX1 expressing MFs had 18-fold (sh2) and sevenfold (sh4) higher β/α collagen compared to control MFs (Fig. 1k).

PRDX1 inactivation in mammary fibroblasts via phosphorylation on Tyr194

Given that MFs deficient in PRDX1 caused dramatic effects to collagen in cell-based assays and in vivo, we next examined how endogenous PRDX1 inactivation occurs in MFs. The PRDX1 gene is rarely affected by genomic alterations in cancer [34]. In breast cancer patient samples, 0.2% had PRDX1 mutations and 1.3%

Fig. 1 Loss of PRDX1 in MFs promotes collagen remodelling in mammary glands of a syngeneic mouse model vivo and MFs in vitro. a shPRDX1-4 or EV MFs were transplanted into fat pads of 8-week-old female BALB/c mice together with GFP+ 67NR breast cancer cells. One week after transplantation, glands were harvested and analysed by multiphoton microscopy. **b** Quantification of collagen intensities. Bars indicate EV (black) or sh (white) for 1 or 2 weeks. **c–g** Second-harmonic generation (SHG) imaging is used to identify collagen fibres which were then analysed using curvelet transformation (CT) and fibre extraction (FIRE) algorithms available through open-source software (see "Materials and methods"). Eight images of eight tumours in four mice for each MF genotype (EV or shPRDX1 MFs, respectively) were analysed. **c** SHG images overlayed with CT-FIRE tracing (right) for collagen length. Statistical test: Student *t* test. **d** Dot plot showing the frequency of average collagen length per image; for EV an average of 903 fibres/image were analysed and for shPRDX1 a total of 996 fibres/image were analysed; Statistical test: Student's *t* test. **e** Dot plot showing significant differences in alignment coefficients in mammary. Statistical test: Student's *t* test. **f** SHG images (overlayed with CT-FIRE tracing for collagen fibre perpendicular angle distribution 0–90°). **g** Histogram showing significant differences in the frequency of angles. $^{*}P < 0.05$; $^{**}P < 0.005$. Statistical test: Student's *t* test; **h** Post mammary gland injection, at weeks 1, 2 and 4, tumour size was measured by calliper. **i** Scrambled control shRNA (scr) or shRNA PRDX1 clones (sh2 or sh4) MFs were plated in a 48-well plate and incubated with 5% CO_2 and 5% O_2 at 37 °C for 6 days. Pepsin-digested samples were separated by SDS-PAGE under non-reducing conditions and silver-stained to compare collagen forms. **j, k** PRDX1-deficient MFs have increased lower molecular weight α-collagen (black), cross-linked higher molecular weight β-collagen (grey) and β/α-collagen ratio. $^{*}P < 0.05$; $^{**}P < 0.005$.

displayed amplifications in the TCGA database, while homozygous gene deletion is not detected (Fig. 2a). This suggested that PRDX1 inactivation most likely occurs posttranslationally. The PRDX1 peroxidase reduces peroxides via a highly conserved cysteine residue (C52) that serves as the site of oxidation by peroxides. Peroxides oxidise this cysteine to sulfenic acid which then reacts with a resolving cysteine (C173) of another PRDX1 protein to form a disulfide that is then subsequently reduced by an appropriate electron donor to complete a catalytic cycle. Much work has been done characterising the regulation of PRDX1 by peroxides, but recent evidence also suggests that other posttranslational modifications such as phosphorylation regulate its peroxidase activity [35]. The crosstalk between different cell types and cancerous stroma is recognised to be essential in cancer progression, with ROS playing an important role in signalling processes in the tumour microenvironment [36]. To test if loss of PRDX1 function in MFs stems from peroxide-mediated inactivation, we examined if cancer cell-mediated ROS participate in the inactivation of PRDX1. While H_2O_2 treatment of MFs showed inactivating over-oxidation of PRDX1 C52, conditioned media (CM) from breast cancer cells (MCF-7 and MDA-MB-231) had no effect on oxidising PRDX1 to the sulfonic acid form (Fig. 2b). A role for PRDX1 has been described in wound healing where growth factor signalling induces PRDX1 phosphorylation on Y194 and thus peroxidase inactivation through SRC [25]. Interestingly, PRDX1-Y194 phosphorylation increased twofold when incubated with CM from MDA-MB-231 cells (Fig. 2c, d). In contrast, CM from MCF-7 cells, stimulation with serum or H_2O_2 had very little effect. As expected, CM from MDA-MB-231 cells, as well as H_2O_2, significantly induces Y416 on SRC (Fig. 2e, f). These findings were further confirmed by incubating MFs with CM from two other TNBC cell lines, MDA-MB-468 and BT-549 (Supplementary Fig. S2A, B). Utilising a widely used SRC inhibitor PP1, we demonstrated that MDA-MB-231 CM treatment with PP1 diminished SRC Y416 phosphorylation as well as PRDX1 phosphorylation on Y194 (Fig. 2g, h). These results suggest a signalling axis induced through paracrine signalling from MDA-MB-231 cancer cells through MF SRC that leads to an inactivation of PRDX1 through Y194 phosphorylation.

PRDX1 regulates ECM collagen cross-linking via lysyl oxidase (LOX)

Lysyl oxidase (LOX) proteins are the primary enzyme responsible for collagen cross-linking in the tumour microenvironment [37]. To determine if increased collagen cross-linking in shPRDX1 MFs is dependent on LOX activity, MFs were treated with βAPN, a widely used LOX family inhibitor that significantly decreased β11 and β12 collagen accompanied by an increase in α1 and α2 collagen (Fig. 3a, b). To further investigate how the loss of PRDX1 function increases collagen bundling in the ECM, intracellular and secreted extracellular LOX were probed. Control and PRDX1-deficient MFs displayed similar levels of intracellular unprocessed LOX protein under non- or starvation conditions (Supplementary Fig. S3C, D), but active extracellular LOX was increased fourfold in media collected from PRDX1-deficient MFs compared to control cells (Fig. 3c, d). This increased secretion could partially be repressed by the pan SRC inhibitor PP1 (~30%), suggesting a role for PRDX1 in decreasing extracellular active LOX through SRC activity (Fig. 3e, f). Whether CM from MDA-MB-231 cells, shown in Fig. 2 to increase the phosphorylation of Y194 PRDX1 to inactivate peroxidase activity, could also increase collagen bundling was next examined. MDA-MB-231 CM increased collagen bundling of MFs sixfold when compared to non-conditioned media. Importantly, LOX secretion was predominately from MFs and not due to cancer cell-secreted LOX within the CM and stimulation of control MFs with CM from MDA-MB-231 cells was able to increase extracellular active LOX protein to levels comparable to those found with shPRDX1 2/4 MFs (Fig. 3g, h).

PRDX1 associates with LOX and LOXL2

PRDX1 has been identified as a promiscuous binding partner for a wide range of signalling proteins such as c-Abl, c-Myc, ASK-1, p66SHC, PTEN, androgen receptor and JNK [13, 38–43]. Thus, it was investigated if the observed increase in extracellular LOX in the absence of PRDX1 in MFs, correlates with PRDX1 binding to LOX proteins. 293T HEK cells were transfected with FLAG-LOX or LOXL2, and FLAG pulldown detected co-immunoprecipitated endogenous PRDX1 in both, H_2O_2-treated and untreated cells (Fig. 4a). Notably, although the oxidised environment created by 100 µM H_2O_2 leads to oxidation of C52 in PRDX1, which can reportedly decrease binding to other proteins [34]. H_2O_2 treatment did not affect PRDX1 binding to LOX proteins. Instead, treatment of cells with CM induced detectable Y194 PRDX1 phosphorylation (Fig. 4b, lysate), but not LOX binding to PRDX1 (Fig. 4b, IP). To better demonstrate the functional significance of Y194 phosphorylation, a Y194 phosphomimetic mutant (Y194D) was examined. As shown in Fig. 4c and d, Y194D PRDX1 proteins expressed in *Prdx1*$^{-/-}$ MFs, increased collagen bundling by 33% compared to *Prdx1*$^{-/-}$ MFs reconstituted with PRDX1 WT protein, thus mimicking collagen bundling found in *Prdx1*$^{-/-}$ MFs. In addition, *Prdx1*$^{-/-}$ Y194D PRDX1 MFs, secreted fivefold more LOX proteins compared to *Prdx1*$^{-/-}$ MFs, reconstituted with WT PRDX1 protein. In summary, these data suggest that phosphorylation of PRDX1 on Y194 abrogate binding of LOX to PRDX1 that correlates with increased extracellular LOX and collagen remodelling (Fig. 4e, f).

PRDX1 and Y416 SRC phosphorylation correlate with patient survival in breast cancer

To examine the role of Y194 PRDX1 phosphorylation translationally, we analysed MFs and mouse mammary glands (PRDX1 WT and KO) by immunofluorescence. Unfortunately, the antibody utilised to detect Y194 phosphorylated PRDX1 by immunoblotting

a

(%)	Mutation	Amplification	Deletion
All BC	0.2	1.3	0
ER+	0.3	0.5	0
ER-	0	5	0
TNBC	0	2.4	0

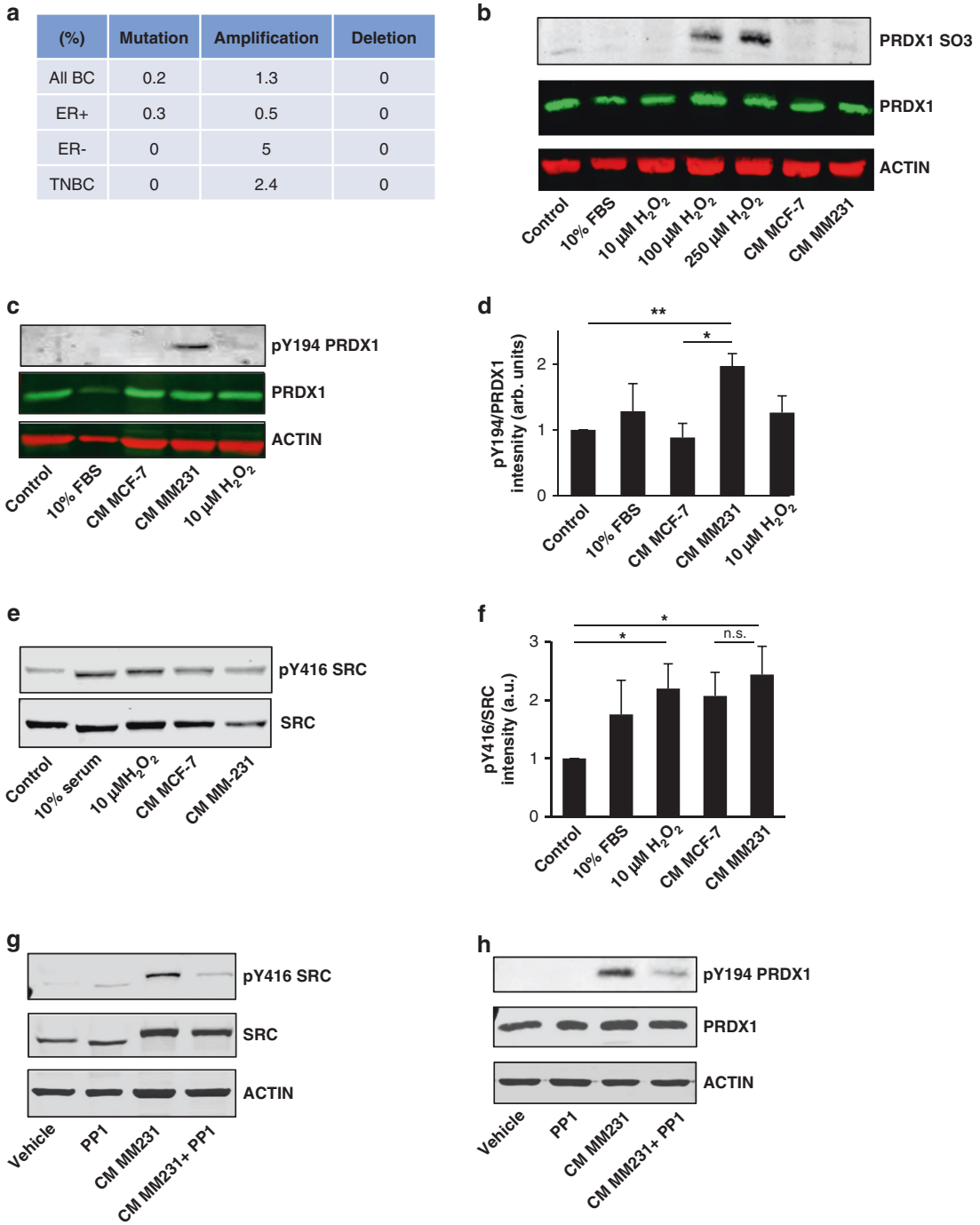

Fig. 2 MDA-MB-231 cancer-conditioned media increases phosphorylation of Y194 PRDX1. a PRDX1 exhibits low levels of mutation, amplification and deletion in TCGA breast cancer samples. **b** Over-oxidation of PRDX1 was probed by immunoblot 30 min following treatment of MFs with 0-250 μM H_2O_2, 10% FBS, or cancer-conditioned media from MCF-7 or MM231 cells. **c**–**f** Immunoblots were probed for phosphorylated Y194 PRDX1 or Y416 from lysates of MFs treated for 30 min with serum-free media, 10 μM H_2O_2, 10% FBS or cancer-conditioned media from MCF-7 or MM231 cells. **g**, **h** MFs were pretreated with or without 20 μM PP1 before treatment with serum-free media or MM231 conditioned media. Lysates were probed by immunoblot for phosphorylated Y194 PRDX1 or Y416. Values represent mean + SEM ($n = 3$). *$P < 0.05$; **$P < 0.005$.

showed unspecific staining patterns in immunofluorescence experiments testing its antigen specificity comparing shPRDX1 and control MFs. No other antibody is currently commercially available. In an attempt to partially circumvent this limitation, datasets containing mRNA or protein analysis were probed. Utilising the Illumina Correlation Engine, tissue-specific expression levels for breast epithelial and breast stroma were analysed. In benign tissue, PRDX1 mRNA in the mammary stroma was 3.25 higher compared to epithelial cells, and in malignant tissues, this difference ranged from 3.65 to 2.39 in two independent datasets (Fig. 5a and Supplementary Table 1). Unfortunately, expression for SRC kinase was not available in these datasets. However, interestingly, while PRDX1 expression was found lower in normal breast stroma compared to cancerous breast stroma ranging from

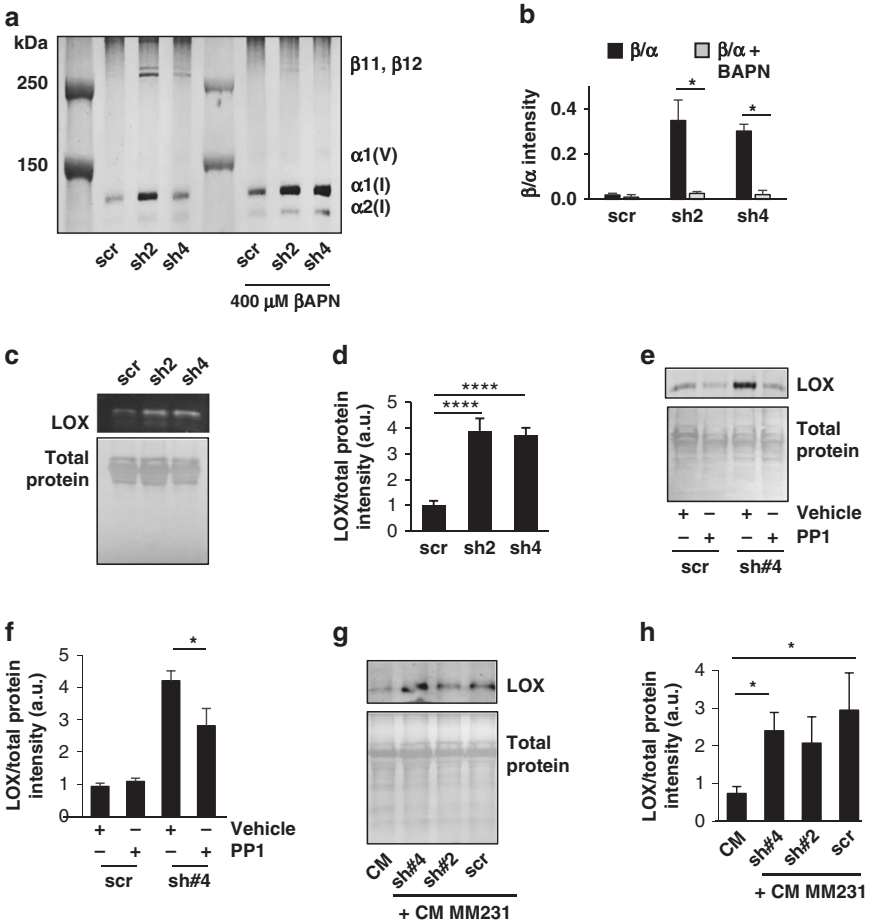

Fig. 3 LOX secretion is increased in PRDX1-deficient and cancer-conditioned media-treated MFs. a, **b** MFs treated with vehicle (black) or 400 μM βAPN (grey) to inhibit LOX family member collagen cross-linking inhibited β-collagen formation. Values represent mean + SEM ($n = 3$). **c**–**h** Scr and PRDX1-deficient MFs were incubated with serum-free media for 24 h then supernatants were precipitated with trichloroacetic acid and sodium deoxycholate. Precipitated extracellular proteins were then probed for LOX by immunoblot and normalised to Ponceau S-stained membranes. **e**, **f** Precipitated supernatants from control or PRDX1-deficient MFs were treated with vehicle or PP1 and probed for LOX by immunoblot. **g**, **h** LOX from supernatants of MM231 conditioned media was compared to control or PRDX1-deficient MFs incubated with MM231 conditioned for 24 h. Values represent mean + SEM ($n = 3$). *$P < 0.05$; **$P < 0.005$.

1.4 up to threefold (three independent datasets, Fig. 5b and Supplementary Table 1), for SRC, the opposite was found: a higher expression of SRC mRNA is present in cancerous stroma compared to normal breast stroma ranging from 2.1 up to 159-fold (Fig. 5b and Supplementary Table 2). Increased PRDX1 mRNA expression has been associated with lower relapse-free survival (RFS) in breast cancer with no effect on overall survival (OS) utilising the KM-plotter tool [44, 45]. Notably, analysing OS of breast cancer patients, depending on PRDX1 protein levels in two independent datasets, showed that, while log-rank survival *P* values are not significant, patients with higher PRDX1 protein expression tend to live longer compared to patients with the lower expression: low expression cohort 70.9 months, high expression cohort 90.4 months (Fig. 5c (TCGA dataset) and S4A (Liu dataset)) [44]. In support of this, analysing OS by selecting patients with low PRDX1 protein expression (one standard deviation below the average expression of the dataset) shows a significant disadvantage for patients with shorter median survival of 107.6 months compared to patients with unchanged PRDX1 expression and a median survival of 130.1 months (Supplementary Fig. S4B) (TCGA, breast cancer, Firehouse Legacy) [46]. Interestingly, while OS of breast cancer patients seems independent of SRC protein levels (Supplementary Fig. S4C), patients with higher levels of Y416 phosphorylated SRC show shorter OS compared to lower expressing breast cancer patients, where the low expression cohort presents with a median survival of 148.53 months and the high expression cohort with a median survival of 115.73 months (Fig. 5d). Collectively these data suggest that PRDX1 is expressed higher in breast stroma compared to breast epithelial cells, and elevated PRDX1 protein levels correlate with longer survival while the opposite is true for Y416 phosphorylated SRC protein, where higher levels correlate with shorter overall survival. Assuming that decreased PRDX1 levels reflect decreased PRDX1 peroxidase activity, we propose that PRDX1 acts as a tumour suppressor in stroma breast cancer tissues. Thus, in conclusion, the following model is proposed: upon activation by H_2O_2, or other stimuli including growth factor receptor or integrin signalling, SRC phosphorylates PRDX1-Y194, which results in the inactivation of PRDX1. PRDX1 binding to LOX is then disrupted, allowing LOX to be secreted to the ECM where it functions to cross-link collagen fibres, resulting in linearised collagen fibrils which have been shown to promote the progression of breast cancer and metastasis (Fig. 5e).

DISCUSSION

The transition of fibroblasts to myofibroblasts during wound healing resembles the transition of stromal mammary fibroblasts into CAFs during cancer development. While during wound healing, growth factor secretion ceases after wound closure when

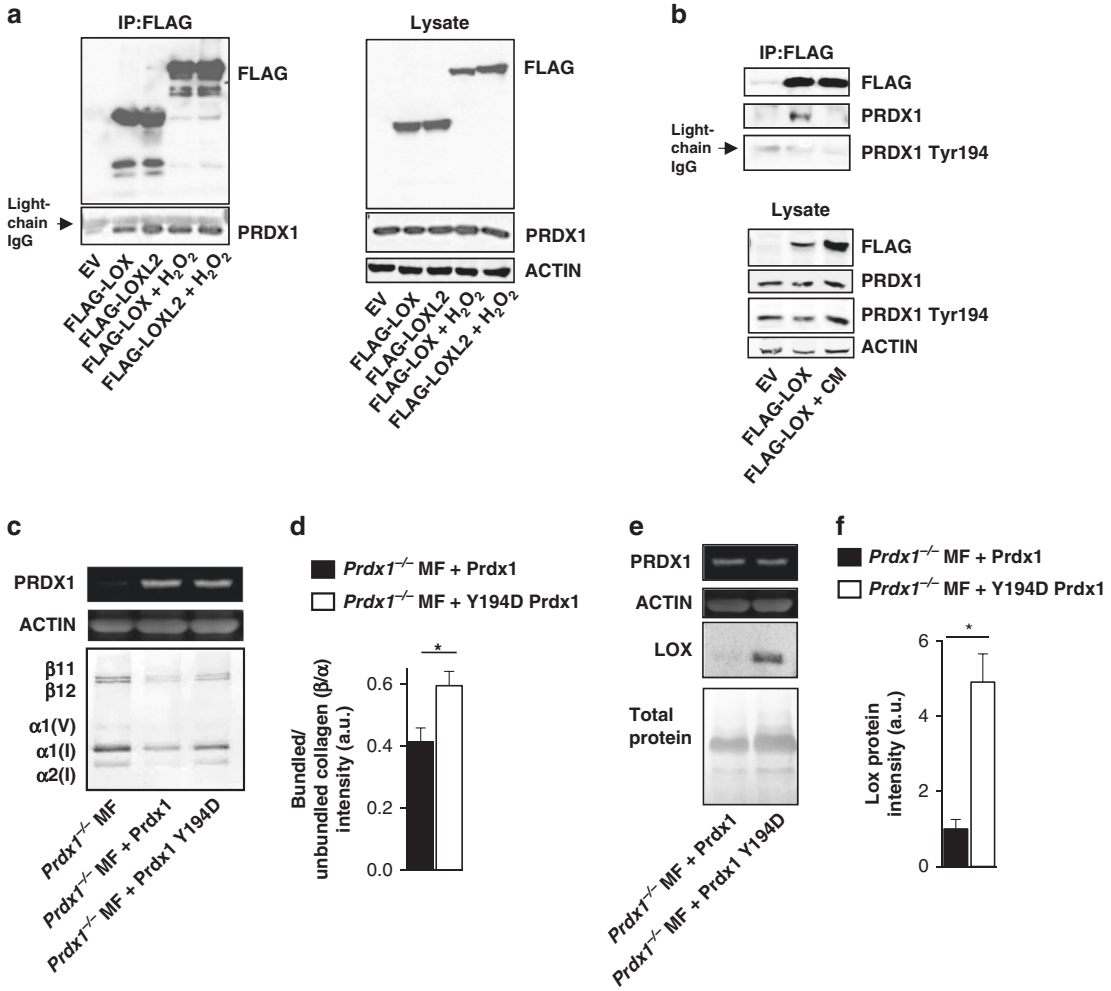

Fig. 4 Prdx1 binds LOX family proteins regulating collagen cross-linking. a, **b** Immunoprecipitations of transiently transfected FLAG-LOX and FLAG-LOXL2 plasmids in HEK 293T treated with 100 μM H_2O_2 or MM231 conditioned media for 30 min immunoblotted for endogenous PRDX1. **a** FLAG-LOX and FLAG-LOXL2 bound PRDX1 in the presence or absence of H_2O_2, but not when treated with MM231 cancer-conditioned media. **c**, **d** *Prdx1*$^{-/-}$ MF were transduced with wild-type PRDX1 or the phosphor-mimetic mutant Y194D PRDX1. MFs were plated in a 48-well plate and incubated with 5% CO_2 and 5% O_2 at 37 °C for 6 days. Silver-stained SDS-PAGE samples of pepsin-digested lysates show wild-type PRDX1 MFs inhibit the bundled to unbundled, β/α-collagen ratio more than Y194D PRXDX1 MFs. **e**, **f** LOX secretion was elevated in *Prdx1*$^{-/-}$ MF expressing Y194D PRDX1 compared to wild-type PRDX1. Values represent mean + SEM ($n = 3$). *$P < 0.05$; **$P < 0.005$.

myofibroblasts die off, during carcinogenesis, fibroblasts remain perpetually exposed to growth factors and other molecules resulting in continuing ECM remodelling and tissue stiffness that supports breast cancer progression [47, 48].

ROS drive the transition of fibroblasts to myofibroblasts and thus play an important role in wound healing and stromal responses mediated by CAFs in cancer [49, 50]. We have recently demonstrated that PRDX1 represses H_2O_2 production in mammary fibroblasts (MFs) and inhibits CAF characteristics, such as motility, invasive properties and the expression of CAF specific markers [15]. Utilising now a syngeneic mouse model where shPRDX1 RNA expressing MFs or control MFs were co-transplanted with 67NR non-aggressive breast cancer cells [16], we report that specific loss of PRDX1 in MFs significantly increases collagen remodelling in murine mammary glands. Many studies have established that collagen cross-linking actively contributes to invasion and metastasis by enhancing ECM stiffness, fibrosis and cancer cell adhesion to the ECM [47, 48]. The effects of collagen remodelling in the presence of PRDX1-lacking MFs were observed as early as 1 week after co-transplantation, supporting the hypotheses that breast cancer cell dissemination is indeed an early event [51]. Architectural rearrangement of collagen in the tumour microenvironment (tumour-associated collagen signature: TACS) is associated with breast cancer patient survival. Three TACS classifications are described with TACS-3 being characterised by bundles of straightened and aligned collagen fibres that are oriented perpendicular to the tumour boundary. Tumours exhibiting TACS-3 are an independent diagnostic factor for poor patient outcome [52, 53]. Lack of PRDX1 MFs increases collagen fibre length, alignment, perpendicular orientation, and a twofold higher TACS-3 in mammary glands co-injected with shPRDX1 MFs compared to control MFs, pointing to a beneficial role for PRDX1 in controlling stroma-rich breast cancers.

The role of PRDX1 in cancer is probably bifunctional. While peroxiredoxins prevent tumorigenesis by protecting the cell from mutagenic oxidative damage [54], the upregulation in cancer has spurred the idea of targeting peroxiredoxins in cancer to combat drug resistance [55]. Alternating roles of PRDX1 in initiation, progression and cell types may explain the phenotypical differences. For example, while xenograft studies utilising breast cancer cells that lack PRDX1 show decreased tumour burden [56], we demonstrate here that there is an important cell-autonomous function for PRDX1 in MFs that regulates lysyl oxidase (LOX)-dependent collagen bundling and thus suggests a breast cancer inhibitory role for

a

Breast epithelium vs breast stroma	GSE10797		GSE14548	
	Normal breast	Invasive breast cancer	Non-invasive breast cancer	Invasive breast cancer
PRDX1	3.25	3.65	2.39	N/A
***P* value**	0.0035	0.0002	0.013	N/A

b

Breast cancer stroma vs normal stroma	GSE9014	GSE26910	GSE14548	
PRDX1	1.68	1.44	2.01*	1.58
***P* value**	0.026	0.016	0.027	0.044
	GSE9014	GSE80333**	GSE8977	
SRC	-3.11	-2.14	-1.53	-159
***P* value**	0.036	3.80E-12	0.017	2.50E-07

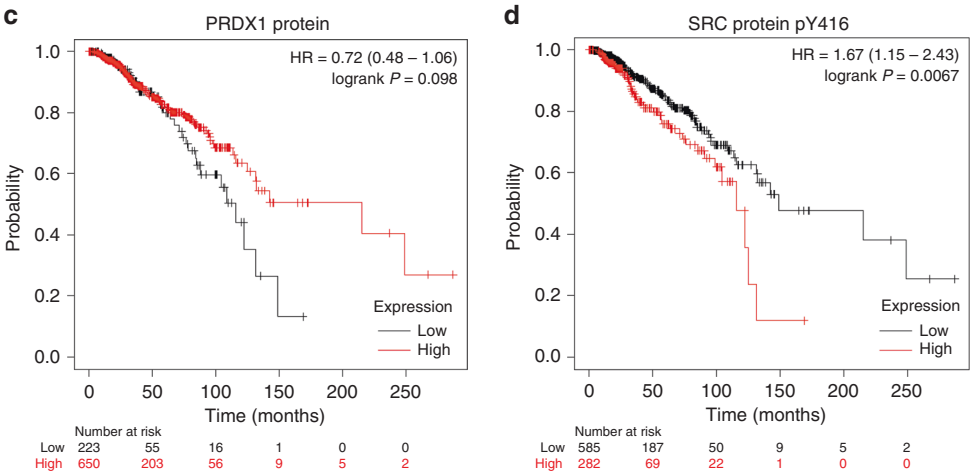

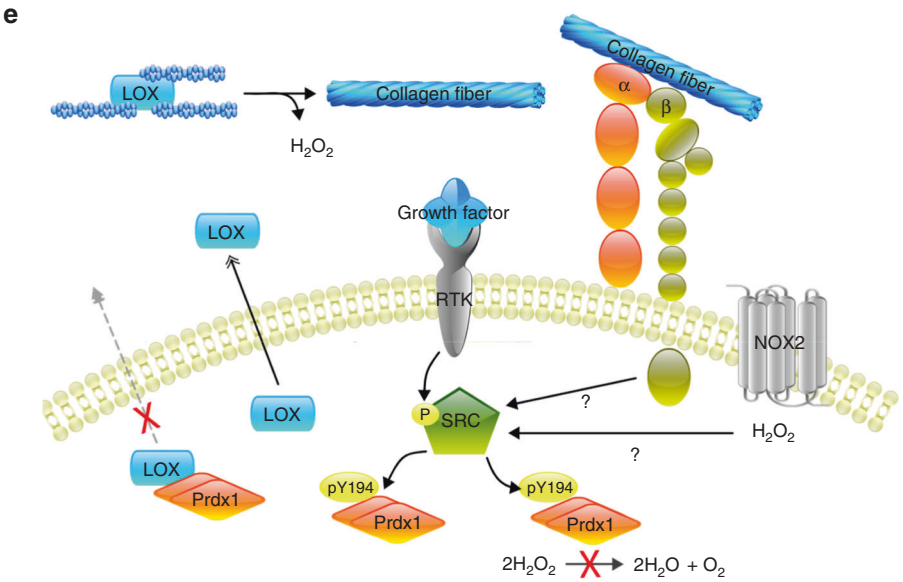

PRDX1. In addition, comparing PRDX1 expression levels in breast tissues using several the NextBio datasets revealed that PRDX1 is several-fold upregulated in stromal tissue compared to epithelial tissue (Supplementary Table 1) and also elevated in normal stroma compared to cancerous breast stroma (Supplementary Table 2). This supports a role for stromal PRDX1 in breast cancer. Overall, this suggests PRDX1 tissue-specific roles in breast cancer.

PRDX1 peroxidase activity relies on the catalytic cysteine (C52) thiolate (S^-) forming a disulfide with the resolving cysteine of another PRDX1 protein (C173) thus reducing $2H_2O_2$ to $2H_2O$ and O_2. Enzymatic reduction through the thioredoxin system then reduces then PRDX1 dimers to monomers prepared for the next catalytic cycle. However, as a consequence of excessive H_2O_2 PRDX1 C52 can undergo over-oxidation to sulfonic acid (SO_3),

Fig. 5 PRDX1 protein levels and SRC Tyr416 protein phosphorylation correlate with the overall survival of breast cancer patients. a, **b** Tissue-specific expression levels for breast epithelial and breast stroma were analysed for PRDX1 and SRC mRNA utilising the Illumina Correlation Engine. **c** Overall survival of breast cancer patients based on PRDX1 protein expression from the TCGA RPPA dataset used in KM plotter. Median survival in low expression cohort 148.5 months and 115.7 months in high expression cohort. **d** Overall survival of breast cancer patients based on SRC Tyr416 phosphorylation levels analysed from the TCGA RPPA dataset used in KM plotter. Median survival in low expression cohort 148.5 months and 215.2 months in high expression cohort. **e** Model of PRDX1-dependent LOX secretion and collagen cross-linking. SRC phosphorylation can occur by either H_2O_2 or growth factor-mediated mechanisms, leading to phosphorylation of PRDX1-Y194, resulting in the inactivation of PRDX1. PRDX1 binding to LOX is then disrupted, allowing LOX to be secreted to the ECM where it functions to cross-link collagen fibres, resulting in linearised collagen fibrils which have been shown to promote the progression of breast cancer and metastasis.

which is an irreversible modification [57, 58]. The vast majority of PRDX-related studies that examine peroxidase linked posttranslational modifications focus on the oxidation of the catalytic cysteine. Recently, however, more studies recognise the importance of other posttranslational modifications, namely phosphorylation [35]. Woo et al. reported that PRDX1 peroxidase activity is transiently inactivated following Y194 phosphorylation due to growth factors such as PDGF and EGF activating the tyrosine kinases SRC. Structural modelling in combination with in vitro data utilising recombinant PRDX1-Y194 mutants demonstrate that Y194F PRDX1 protein is capable of scavenging H_2O_2, while the phosphomimetic Y194D PRDX1 protein is unable to because it lacks peroxidase activity. This led to the following hypothesis: the phosphate moiety of phospho-Y194 of one subunit of the PRDX1 homodimer is positioned within 9 Å of the sulfur atom of the C52 of the other subunit. The negatively charged phosphate group is thus expected to impair the deprotonation of the C52 and therefore its reactivity with H_2O_2 [25]. These data support our finding of absent inactivating over-oxidation of PRDX1 C52 by conditioned media (CM) from breast cancer cells (MCF-7 and MDA-MB-231). Phosphorylation of Y194 diminishes the PRDX1 interaction with LOX proteins. It is therefore possible, that C52 deprotonation is required for PRDX1 binding with LOX proteins. This hypothesis is currently being tested.

We demonstrate that Y194 PRDX1 phosphorylation is induced by adding breast cancer cell-conditioned media to MFs and is greatly diminished by the SRC inhibitor PP1. As this inhibitor is also acting on other SRC-kinase family members such as LCK, FYN and HCK, future studies need to determine which other PP1 targets contribute to PRDX1-Y194 phosphorylation in MFs. SRC kinase is a well-described oncogene. Recent studies convincingly demonstrate SRC can drive pathological processes in fibrosis including extracellular collagen deposition and remodelling, and myofibroblast differentiation [59]. Given the similarities between CAFs and fibrosis-related fibroblasts, a role for SRC in remodelling and fibrosis supports our findings here. The SRC inhibitor Nintedanib has recently been proven to significantly improve idiopathic pulmonary fibrosis in Phase 3 clinical trial [60]. In addition, LOX proteins are also considered potential therapeutic targets in pulmonary fibrosis [61].

A LOX-SRC activation axis has been described where LOX-mediated collagen cross-linking can activate SRC, suggesting a positive feedback loop between extracellular collagen cross-linking and intracellular SRC activation in MFs [62]. Our findings support these data as the pan SRC inhibitor PP1 does not inhibit LOX secretion in control MFs and only in PRDX1-deficient MFs suggesting that the lack of PRDX1 function contributes to SRC-induced LOX activation. Nevertheless, PP1 only decreased LOX secretion by ~30% in PRDX1-deficient MFs, suggesting that other kinases may contribute to Y194 phosphorylation. Abl may be one of these kinases as recent findings identified PRDX1 as an Abl-binding partner and probable target [25, 43]. Along those lines, the LOX-SRC axis itself may explain the rather small difference in collagen bundling between wild-type PRDX1 and Y194D PRDX1 mutant expressing MFs, as the reconstituted wild-type PRDX1 protein is possibly inactivated by SRC-induced phosphorylation during the 6-day collagen deposition assay compared to the shorter one-day LOX secretion assay. The collagen bundling differences may also be affected by the fact that re-expression of Prdx1 in *Prdx1*$^{-/-}$ MF does not seem to fully diminish β-collagen to levels as low as those seen in WT MF in Figs. 1i and 3a. This would suppress the differences in β to α collagen levels when comparing Prdx1 and Y194D Prdx1 mutant rescue MF and suggests Prdx1 rescue expression in *Prdx1*$^{-/-}$ MF is incomplete. Another possible contributor to this result could be the lack of ascorbic acid in the culture media [63] known to be an important co-factor for hydroxylation of peptide-bound proline needed for collagen secretion [64]. As LOX secretion is fivefold higher when the PRDX1-Y194 mimetic is expressed, higher amounts of secreted collagen would likely confer a bigger difference in collagen bundling between the PRDX1 Y194D mutant and PRDX1 WT reconstituted MFs.

In recent years, many studies have highlighted the important role of crosstalk between cancer cells and CAFs [65]. We demonstrate SRC activation in MFs by exposing cells to CM from several human TNBC cell lines. While our analysis does not define the stimulant in the conditioned medium that induces SRC activity, several proteomic analyses of TNBC cell line CM show enrichment of known SRC activators, such as growth factors and integrins [66, 67]. Future studies are needed to specify the activators of SRC-family members responsible for PRDX1-Y194 phosphorylation. It is noteworthy that, while the addition of MCF-7 CM to MFs resulted in SRC Y416 phosphorylation, PRDX1-Y194 phosphorylation was not detectable. Although this might suggest a BC-subtype specific response, more analysis is warranted to test this hypothesis.

CAF populations change during breast cancer progression. An unbiased approach identified eight CAF subtypes in two main CAF populations, pCAFs and sCAFs, based on selective expression of the markers *Pdpn* or *S100a4* (FSP1), respectively [68]. Similar to our study, the syngeneic BALB/c mouse model was used where TNBC mouse 4T1 cells (the aggressive counterpart to 67NR cells) were transplanted into mammary glands. Fibroblasts were then sampled 2 and 4 weeks following cell injection as well as after spontaneous metastasis formation. In support of the data shown here, it was found that pCAFs' expression patterns included wound healing genes such as *α-SMA, TIMP1, LOX, Col1a1* at the earlier 2-week timepoint [68]. This supports our data where PRDX1 loss in MFs promotes CAF-like wound healing responses after 1 and 2 weeks in vivo. Further translational importance can be observed from human breast cancer survival analysis in which pCAFs and sCAF BALB/c expression pattern-subtyping was used to separate patient populations. High positive staining of stromal PDPN proteins significantly correlated with shorter recurrence-free survival, and a low S100a4/high PDPN stromal protein staining specifically associated with shorter survival of *BRCA*-mutant TNBC breast cancer patients [68].

In conclusion, we highlight a novel role for PRDX1 in collagen remodelling that is regulated by SRC-mediated phosphorylation on Y194 PRDX1 which in turn results in PRDX1 dissociation from LOX and LOXL2 proteins. Loss of PRDX1 or expression of a Y194 mimetic increases extracellular LOX and cross-linking, which in

turn is known to activate SRC kinases. If PRDX1-Y194 phosphorylation correlates with cancer-promoting stromal responses in humans needs to be addressed in future studies.

DATA AVAILABILITY

Data will be available as needed.

REFERENCES

1. Siegel RL, Miller KD, Jemal A. Cancer statistics, 2020. CA Cancer J Clin. 2020;70:7–30.
2. Cirri P, Chiarugi P. Cancer-associated-fibroblasts and tumour cells: a diabolic liaison driving cancer progression. Cancer Metastasis Rev. 2012;31:195–208.
3. Friedl P, Locker J, Sahai E, Segall JE. Classifying collective cancer cell invasion. Nat. Cell Biol. 2012;14:777–83.
4. Shiga K, Hara M, Nagasaki T, Sato T, Takahashi H, Takeyama H. Cancer-associated fibroblasts: their characteristics and their roles in tumor growth. Cancers (Basel). 2015;7:2443–58.
5. Mittal M, Siddiqui MR, Tran K, Reddy SP, Malik AB. Reactive oxygen species in inflammation and tissue injury. Antioxid Redox Signal. 2014;20:1126–67.
6. Li B, Wang JH. Fibroblasts and myofibroblasts in wound healing: force generation and measurement. J Tissue Viability. 2011;20:108–20.
7. Byun JS, Gardner K. Wounds that will not heal: pervasive cellular reprogramming in cancer. Am J Pathol. 2013;182:1055–64.
8. Dvorak HF. Tumors: wounds that do not heal. Similarities between tumor stroma generation and wound healing. N Engl J Med. 1986;315:1650–9.
9. Xiao Q, Ge G. Lysyl oxidase, extracellular matrix remodeling and cancer metastasis. Cancer Microenviron. 2012;5:261–73.
10. Grimsby JL, Lucero HA, Trackman PC, Ravid K, Kagan HM. Role of lysyl oxidase propeptide in secretion and enzyme activity. J Cell Biochem. 2010;111:1231–43.
11. Rhee SG, Woo HA, Kang D. The role of peroxiredoxins in the transduction of H_2O_2 signals. Antioxid Redox Signal. 2018;28:537–57.
12. Skoko JJ, Attaran S, Neumann CA. Signals getting crossed in the entanglement of redox and phosphorylation pathways: phosphorylation of peroxiredoxin proteins sparks cell signaling. Antioxidants. 2019;8:29.
13. Cao J, Schulte J, Knight A, Leslie NR, Zagozdzon A, Bronson R, et al. Prdx1 inhibits tumorigenesis via regulating PTEN/AKT activity. EMBO J. 2009;28:1505–17.
14. Neumann CA, Krause DS, Carman CV, Das S, Dubey DP, Abraham JL, et al. Essential role for the peroxiredoxin Prdx1 in erythrocyte antioxidant defence and tumour suppression. Nature. 2003;424:561–5.
15. Jezierska-Drutel A, Attaran S, Hopkins BL, Skoko JJ, Rosenzweig SA, Neumann CA. The peroxidase PRDX1 inhibits the activated phenotype in mammary fibroblasts through regulating c-Jun N-terminal kinases. BMC Cancer. 2019;19:812.
16. Aslakson CJ, Miller FR. Selective events in the metastatic process defined by analysis of the sequential dissemination of subpopulations of a mouse mammary tumor. Cancer Res. 1992;52:1399–405.
17. Tuer AE, Krouglov S, Prent N, Cisek R, Sandkuijl D, Yasufuku K, et al. Nonlinear optical properties of type I collagen fibers studied by polarization dependent second harmonic generation microscopy. J Phys Chem B. 2011;115:12759–69.
18. Bredfeldt JS, Liu Y, Conklin MW, Keely PJ, Mackie TR, Eliceiri KW. Automated quantification of aligned collagen for human breast carcinoma prognosis. J Pathol Inf. 2014;5:28.
19. Bredfeldt JS, Liu Y, Pehlke CA, Conklin MW, Szulczewski JM, Inman DR, et al. Computational segmentation of collagen fibers from second-harmonic generation images of breast cancer. J Biomed Opt. 2014;19:16007.
20. Liu Y, Keikhosravi A, Mehta GS, Drifka CR, Eliceiri KW. Methods for quantifying fibrillar collagen alignment. Methods Mol Biol. 2017;1627:429–51.
21. Wan L, Skoko J, Yu J, Ozdoganlar OB, LeDuc PR, Neumann CA. Mimicking embedded vasculature structure for 3D cancer on a chip approaches through micromilling. Sci Rep. 2017;7:16724.
22. Lareu RR, Arsianti I, Subramhanya HK, Yanxian P, Raghunath M. In vitro enhancement of collagen matrix formation and crosslinking for applications in tissue engineering: a preliminary study. Tissue Eng. 2007;13:385–91.
23. Lareu RR, Subramhanya KH, Peng Y, Benny P, Chen C, Wang Z, et al. Collagen matrix deposition is dramatically enhanced in vitro when crowded with charged macromolecules: the biological relevance of the excluded volume effect. FEBS Lett. 2007;581:2709–14.
24. Koontz L. TCA precipitation. Methods Enzymol. 2014;541:3–10.
25. Woo HA, Yim SH, Shin DH, Kang D, Yu DY, Rhee SG. Inactivation of peroxiredoxin I by phosphorylation allows localized H(2)O(2) accumulation for cell signaling. Cell. 2010;140:517–28.
26. Chan JS, Tan MJ, Sng MK, Teo Z, Phua T, Choo CC, et al. Cancer-associated fibroblasts enact field cancerization by promoting extratumoral oxidative stress. Cell Death Dis. 2017;8:e2562.
27. Giannoni E, Bianchini F, Calorini L, Chiarugi P. Cancer associated fibroblasts exploit reactive oxygen species through a proinflammatory signature leading to epithelial mesenchymal transition and stemness. Antioxid Redox Signal. 2011;14:2361–71.
28. Jezierska-Drutel A, Rosenzweig SA, Neumann CA. Role of oxidative stress and the microenvironment in breast cancer development and progression. Adv Cancer Res. 2013;119:107–25.
29. Martinez-Outschoorn UE, Balliet RM, Rivadeneira DB, Chiavarina B, Pavlides S, Wang C, et al. Oxidative stress in cancer associated fibroblasts drives tumor-stroma co-evolution: a new paradigm for understanding tumor metabolism, the field effect and genomic instability in cancer cells. Cell Cycle. 2010;9:3256–76.
30. Scholer-Dahirel A, Costa A, Mechta-Grigoriou F. Control of cancer-associated fibroblast function by oxidative stress: a new piece in the puzzle. Cell Cycle. 2013;12:2169.
31. Toullec A, Gerald D, Despouy G, Bourachot B, Cardon M, Lefort S, et al. Oxidative stress promotes myofibroblast differentiation and tumour spreading. EMBO Mol Med. 2010;2:211–30.
32. Hanley CJ, Noble F, Ward M, Bullock M, Drifka C, Mellone M, et al. A subset of myofibroblastic cancer-associated fibroblasts regulate collagen fiber elongation, which is prognostic in multiple cancers. Oncotarget. 2016;7:6159–74.
33. Schedin P, Keely PJ. Mammary gland ECM remodeling, stiffness, and mechanosignaling in normal development and tumor progression. Cold Spring Harb Perspect Biol. 2011;3:a003228.
34. Hampton MB, Vick KA, Skoko JJ, Neumann CA. Peroxiredoxin involvement in the initiation and progression of human cancer. Antioxid. Redox Signal. 2018;28:591–608.
35. Rhee SG, Woo HA. Multiple functions of 2-Cys peroxiredoxins, I and II, and their regulations via post-translational modifications. Free Radic Biol Med. 2020;152:107–15.
36. Weinberg F, Ramnath N, Nagrath D. Reactive oxygen species in the tumor microenvironment: an overview. Cancers. 2019;11:1191.
37. Levental KR, Yu H, Kass L, Lakins JN, Egeblad M, Erler JT, et al. Matrix crosslinking forces tumor progression by enhancing integrin signaling. Cell. 2009;139:891–906.
38. Chhipa RR, Lee KS, Onate S, Wu Y, Ip C. Prx1 enhances androgen receptor function in prostate cancer cells by increasing receptor affinity to dihydrotestosterone. Mol Cancer Res. 2009;7:1543–52.
39. Gertz M, Fischer F, Leipelt M, Wolters D, Steegborn C. Identification of peroxiredoxin 1 as a novel interaction partner for the lifespan regulator protein p66Shc. Aging. 2009;1:254–65.
40. Kim SY, Kim TJ, Lee KY. A novel function of peroxiredoxin 1 (Prx-1) in apoptosis signal-regulating kinase 1 (ASK1)-mediated signaling pathway. FEBS Lett. 2008;582:1913–8.
41. Kim YJ, Lee WS, Ip C, Chae HZ, Park EM, Park YM. Prx1 suppresses radiation-induced c-Jun NH2-terminal kinase signaling in lung cancer cells through interaction with the glutathione S-transferase Pi/c-Jun NH2-terminal kinase complex. Cancer Res. 2006;66:7136–42.
42. Mu ZM, Yin XY, Prochownik EV. Pag, a putative tumor suppressor, interacts with the Myc Box II domain of c-Myc and selectively alters its biological function and target gene expression. J Biol Chem. 2002;277:43175–84.
43. Wen ST, Van Etten RA. The PAG gene product, a stress-induced protein with antioxidant properties, is an Abl SH3-binding protein and a physiological inhibitor of c-Abl tyrosine kinase activity. Genes Dev. 1997;11:2456–67.
44. Nagy A, Lanczky A, Menyhart O, Gyorffy B. Validation of miRNA prognostic power in hepatocellular carcinoma using expression data of independent datasets. Sci Rep. 2018;8:9227.
45. Wang G, Zhong WC, Bi YH, Tao SY, Zhu H, Zhu HX, et al. The prognosis of peroxiredoxin family in breast cancer. Cancer Manag Res. 2019;11:9685–99.
46. Cerami E, Gao J, Dogrusoz U, Gross BE, Sumer SO, Aksoy BA, et al. The cBio cancer genomics portal: an open platform for exploring multidimensional cancer genomics data. Cancer Discov. 2012;2:401–4.
47. Egeblad M, Rasch MG, Weaver VM. Dynamic interplay between the collagen scaffold and tumor evolution. Curr Opin Cell Biol. 2010;22:697–706.
48. Kechagia JZ, Ivaska J, Roca-Cusachs P. Integrins as biomechanical sensors of the microenvironment. Nat Rev Mol Cell Biol. 2019;20:457–73.
49. Alili L, Sack M, Puschmann K, Brenneisen P. Fibroblast-to-myofibroblast switch is mediated by NAD(P)H oxidase generated reactive oxygen species. Biosci Rep. 2014;34:e00089.
50. Sahai E, Astsaturov I, Cukierman E, DeNardo DG, Egeblad M, Evans RM, et al. A framework for advancing our understanding of cancer-associated fibroblasts. Nat Rev Cancer. 2020;20:174–86.
51. Hosseini H, Obradovic MMS, Hoffmann M, Harper KL, Sosa MS, Werner-Klein M, et al. Early dissemination seeds metastasis in breast cancer. Nature. 2016;540:552–8.
52. Conklin MW, Eickhoff JC, Riching KM, Pehlke CA, Eliceiri KW, Provenzano PP, et al. Aligned collagen is a prognostic signature for survival in human breast carcinoma. Am J. Pathol. 2011;178:1221–32.

53. Tomko LA, Hill RC, Barrett A, Szulczewski JM, Conklin MW, Eliceiri KW, et al. Targeted matrisome analysis identifies thrombospondin-2 and tenascin-C in aligned collagen stroma from invasive breast carcinoma. Sci Rep. 2018;8:12941.
54. Nystrom T, Yang J, Molin M. Peroxiredoxins, gerontogenes linking aging to genome instability and cancer. Genes Dev. 2012;26:2001–8.
55. Nicolussi A, D'Inzeo S, Capalbo C, Giannini G, Coppa A. The role of peroxiredoxins in cancer. Mol Clin Oncol. 2017;6:139–53.
56. Bajor M, Zych AO, Graczyk-Jarzynka A, Muchowicz A, Firczuk M, Trzeciak L, et al. Targeting peroxiredoxin 1 impairs growth of breast cancer cells and potently sensitises these cells to prooxidant agents. Br J Cancer. 2018;119:873–84.
57. Lim JC, Choi H-I, Park YS, Nam HW, Woo HA, Kwon K-S, et al. Irreversible oxidation of the active-site cysteine of peroxiredoxin to cysteine sulfonic acid for enhanced molecular chaperone activity. J Biol Chem. 2008;283:28873–80.
58. Woo HA, Chae HZ, Hwang SC, Yang KS, Kang SW, Kim K, et al. Reversing the inactivation of peroxiredoxins caused by cysteine sulfinic acid formation. Science. 2003;300:653–6.
59. Li H, Zhao C, Tian Y, Lu J, Zhang G, Liang S, et al. SRC family kinases and pulmonary fibrosis: a review. Biomed. Pharmacother. 2020;127:110183.
60. Flaherty KR, Wells AU, Cottin V, Devaraj A, Walsh SLF, Inoue Y, et al. Nintedanib in progressive fibrosing interstitial lung diseases. N Engl J Med. 2019;381:1718–27.
61. Chen L, Li S, Li W. LOX/LOXL in pulmonary fibrosis: potential therapeutic targets. J Drug Target. 2019;27:790–6.
62. Cox TR, Bird D, Baker AM, Barker HE, Ho MW, Lang G, et al. LOX-mediated collagen crosslinking is responsible for fibrosis-enhanced metastasis. Cancer Res. 2013;73:1721–32.
63. Azqueta A, Costa S, Lorenzo Y, Bastani NE, Collins AR. Vitamin C in cultured human (HeLa) cells: lack of effect on DNA protection and repair. Nutrients. 2013;5:1200–17.
64. The function of ascorbic acid in collagen formation. Nutr Rev. 1978;36:118–21.
65. da Cunha BR, Domingos C, Stefanini ACB, Henrique T, Polachini GM, Castelo-Branco P, et al. Cellular interactions in the tumor microenvironment: the role of secretome. J Cancer. 2019;10:4574–87.
66. Alghanem B, Ali R, Nehdi A, Al Zahrani H, Altolayyan A, Shaibah H, et al. Proteomics profiling of KAIMRC1 in comparison to MDA-MB231 and MCF-7. Int J Mol Sci. 2020;21:4328.
67. Kulasingam V, Diamandis EP. Proteomics analysis of conditioned media from three breast cancer cell lines: a mine for biomarkers and therapeutic targets. Mol Cell Proteom. 2007;6:1997–2011.
68. Friedman Gil, L-G O, David Eyal, Bornstein Chamutal, Giladi Amir, Dadiani Maya, et al. Cancer-associated fibroblast compositions change with breast cancer progression linking the ratio of S100A4+ and PDPN+ CAFs to clinical outcome. Nat Cancer. 2020;1:692–708.

ACKNOWLEDGEMENTS

The results shown here are in whole or part based upon data generated by the TCGA Research Network: https://www.cancer.gov/tcga. Flow Cytometry Cell Sorting was performed by Joan Brozick at the Flow Cytometry Core on a BD FACSAria Fusion system. The Flow Core is supported by contributions from generous philanthropists through the MWRI Foundation of Pittsburgh, PA.

AUTHOR CONTRIBUTIONS

SA, JS and CN designed, performed analysed and interpreted experiments and wrote the manuscript. BH, LW and MW performed experiments. HW and AF interpreted the data.

FUNDING INFORMATION

This work was supported by R01 CA131350 (CAN), CDMRP/BCRP BC095803 (CAN), Howard Hughes Medical Institute Gilliam Predoctoral fellowship PREDC 59008467 (SA), P30-DK072506, (UPMC Hillman Cancer Center), Cotswold Foundation post-doctoral fellowship (JS). This funding body had no role in the design of the study or collection analysis, and interpretation of data and in writing the manuscript.

ETHICS APPROVAL AND CONSENT TO PARTICIPATE

Not applicable.

CONSENT TO PUBLISH

Not applicable.

COMPETING INTERESTS

The authors declare no competing interests.

ADDITIONAL INFORMATION

Supplementary information The online version contains supplementary material available at https://doi.org/10.1038/s41416-021-01510-x.

Correspondence and requests for materials should be addressed to C.A.N.

Reprints and permission information is available at http://www.nature.com/reprints

Publisher's note Springer Nature remains neutral with regard to jurisdictional claims in published maps and institutional affiliations.